AGU PUBLICATIONS

Earth's Future

RESEARCH ARTICLE
10.1002/2016EF000508

A new approach to projecting 21st century sea-level changes and extremes

Philip Goodwin[1], Ivan D. Haigh[1], Eelco J. Rohling[1,2], and Aimée Slangen[3,4]

[1]Ocean and Earth Science, University of Southampton, National Oceanography Centre Southampton, Southampton, UK, [2]Research School of Earth Sciences, The Australian National University, Canberra, Australian Capital Territory, Australia, [3]Institute for Marine and Atmospheric Research Utrecht (IMAU), University of Utrecht, Utrecht, The Netherlands, [4]Royal Netherlands Institute for Sea Research (NIOZ), Department of Estuarine & Delta Systems, Yerseke, The Netherlands

Key Points:
- A novel hybrid approach to projecting sea-level rise is presented, and embedded within an efficient conceptual Earth system model
- Our computationally efficient approach generates probabilistic projections of future sea-level rise, based on historic constraints
- The frequency of extreme sea level events will increase by 1.5 to 8 times more than for previous sea level projections

Corresponding author:
P. Goodwin, p.a.goodwin@soton.ac.uk

Citation:
Goodwin, P., I. D. Haigh, E. J. Rohling, and A. Slangen (2017), A new approach to projecting 21st century sea-level changes and extremes, *Earth's Future*, *5*, 240–253, doi:10.1002/2016EF000508.

Received 25 NOV 2016
Accepted 26 JAN 2017
Accepted article online 30 JAN 2017
Published online 24 FEB 2017

Abstract Future increases in flooding potential around the world's coastlines from extreme sea level events is heavily dependent on projections of future global mean sea level (GMSL) rise. Yet, the two main approaches for projecting 21st century GMSL rise—i.e., process-based versus semi-empirical—give inconsistent results. Here, a novel hybrid approach to GMSL projection, containing a process-based thermosteric contribution and a semi-empirical ice-melt contribution, is embedded within a conceptual Earth system model (ESM). The ESM is run 10 million times with random perturbations to multiple parameters, and future projections are made only from the simulations that are historically consistent. The projections from our hybrid approach are found to be consistent with the dominant process-based GMSL projections from the Climate Model Intercomparison Project phase 5 (CMIP5) ensemble, in that our future ensemble-mean projections lie within ±2 cm of CMIP5 for the end of the 21st century when CMIP5-simulated histories are used to constrain our approach. However, when observations are used to provide the historic constraints for our hybrid approach, we find higher ice-melt sensitivity and additional ensemble-mean GMSL rise of around 13–16 cm by the end of the century. We assess the impact of this additional GMSL rise, projected from observation-consistency, on the increase in frequency of extreme sea level events for 220 coastal tide-gauge sites. Accounting for regional effects, we infer a 1.5–8 times increase in the frequency of extreme sea-level events for our higher GMSL projections relative to CMIP5.

1. Introduction

Twenty-first century sea-level rise projections are currently obtained by means of two main approaches: semi-empirical and process-based/mechanistic. Semi-empirical projections assume that the total combined rate of global mean sea level (GMSL) rise has some fixed sensitivity over time to either global mean surface warming [e.g., *Rahmstorf*, 2007; *Vermeer and Rahmstorf*, 2009], or anthropogenic radiative forcing (using Intergovernmental Panel on Climate Change [IPCC] scenarios) [e.g., *Jevrejeva et al.*, 2012]. The approach then constrains the semi-empirical coefficients of proportionality using historical observations of GMSL rise, and applies these coefficients to construct 21st century GMSL rise projections [e.g., *Rahmstorf*, 2007; *Vermeer and Rahmstorf*, 2009; *Jevrejeva et al.*, 2012; *Rahmstorf et al.*, 2012] based on assumed or modeled trajectories of future warming [e.g., *Collins et al.*, 2013] or radiative forcing [e.g., *Meinshausen et al.*, 2011]. For semi-empirical methods that do not explicitly de-couple the thermosteric and ice volume contributions to sea-level change, future GMSL rise may be overestimated since the ocean heat uptake efficiency per unit warming is likely to decline in the future [*Church et al.*, 2013]. Also, it is unclear whether the sensitivity of the ice volume component of sea-level rise will be constant with regard to rising temperatures over time, given that the areas of the ice sheets and glaciers that are currently most susceptible to melting will disappear in the future [*Church et al.*, 2013; *Rahmstorf et al.*, 2012].

Process-based sea-level projections derive from representations of ocean thermal expansion, the hydrosphere and the cryosphere, which are either represented within Earth system models (ESMs) or are calculated off-line forced by ESM climatological output [e.g., *Church et al.*, 2013; *Marzeion et al.*, 2012; *Flato et al.*, 2013]. Currently, the Coupled Model Intercomparison Project phase 5 (CMIP5) ensemble of complex mechanistic climate models is the dominant suite used for future sea-level projections [*Church et al.*, 2013] (Figure 1, black). Process-based models solve for sea-level rise over time in response to simulated climate changes, although not all processes are resolved, especially those acting on small spatial scales, and some

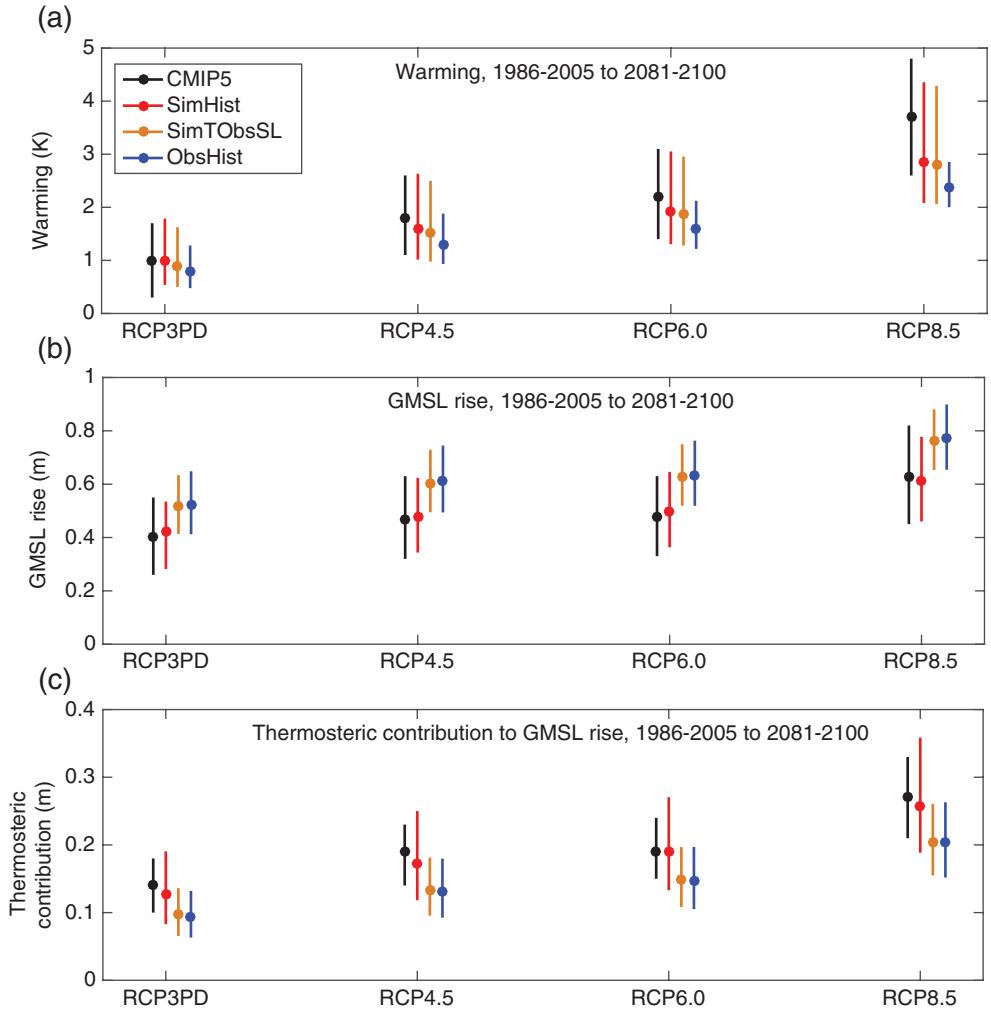

Figure 1. Future warming and sea level projections from four model ensembles. Projected changes from 1986–2005 to 2081–2100 for four Representative Concentration Pathway (RCP) scenarios for (a) warming, (b) global mean sea level (GMSL) rise, and (c) thermosteric contribution to GMSL rise. The ensemble means (dots) and 5th to 95th percentile ranges (lines) are shown for the Climate Model Intercomparison Project phase 5 (CMIP5) ensemble (black), the *SimHist* ensemble (red), *SimTObsSL* ensemble (orange), and the *ObsHist* ensemble (blue).

processes may be solved off-line from the climate simulations including ice-melt contributions to sea-level rise. By explicitly representing different processes, process-based projections both avoid any assumptions that the GMSL rise sensitivity to forcing remains constant through time, and are able to de-couple different component contributions to sea-level rise.

However, future climate forcing is projected to extend well outside the range of historical forcing [*Meinshausen et al.*, 2011; *Collins et al.*, 2013]. In consequence, even process-based models that manage to accurately simulate historical GMSL rise may be affected by incorrect (or omitted) representations of processes that will become significant for future GMSL rise [*deConto and Pollard*, 2016]. Moreover, the CMIP5-simulated ranges of historical warming [*Flato et al.*, 2013] and sea-level rise [*Church et al.*, 2013] may overlap with those in historical observations [*Hartmann et al.*, 2013], but the agreement is not perfect. The existence of such discrepancies in comparisons for the past suggests that bias may also exist in projections for the future. Finally, the computational cost involved precludes generation of ensembles of thousands of runs with such models, as would be needed for well-defined probabilistic assessments of future changes. Instead, the CMIP5-based ensemble comprises only a few tens of members. Various studies have incorporated input from the limited number of CMIP5 projections to produce full probability density functions of future GMSL rise [e.g.,

Jevrejeva et al., 2014; *Kopp et al.*, 2014; *Grinsted et al.*, 2015], although these studies also utilize expert elicitation among other techniques.

While many semi-empirical analyses yield higher upper projections of GMSL rise than process-based calculations [e.g., *Rahmstorf,* 2007; *Vermeer and Rahmstorf*, 2009; *Jevrejeva et al.*, 2012; *Rahmstorf et al.*, 2012], a recent study by *Kopp et al.* [2016] employed a longer time-series of temperature and sea-level proxy estimates to construct projections to 2100 that agree well with the CMIP5 ensemble [*Church et al.*, 2013]. However, the semi-empirical approach of *Kopp et al.* [2016] still assumes that the overall net rate of sea-level rise from all processes is related linearly to a temperature anomaly, with a constant sensitivity over time. Since this assumption is not inherent within the process-based projections, it remains unclear why the two methods should agree.

In this paper, we present a new hybrid approach to projecting 21st century sea-level rise that complements existing approaches. This new hybrid approach combines a mechanistic representation of thermosteric sea-level rise [*Williams et al.*, 2012] with a semi-empirical representation of the ice volume component of sea-level rise [*Rahmstorf*, 2007], embedded within an efficient conceptual ESM [*Goodwin*, 2016]. This new approach: generates enough ensemble members to form a frequency distribution of future GMSL rise without requiring any additional information, for example, from expert elicitation; explicitly separates out the thermosteric contribution from the ice-melt contribution to GMSL rise; and requires no off-line analysis outside the conceptual ESM simulations. Using GMSL projections from this new approach, we assess impacts on the frequency of extreme sea-level events at 220 tide-gauge sites around the world.

The structure of the paper is as follows. Section 2 describes the methods used to produce GMSL rise projections, and assesses impacts on the frequency of extreme sea-level events at 220 coastal cities. First, the hybrid approach to simulate GMSL is presented, and embedded within an efficient conceptual ESM. Then, the method is described that is used to produce a large Monte Carlo ensemble, from which historically consistent subsets are then extracted. Last, the method used to assess changes in the frequency of extreme events is described. Section 3 presents the results of this study, and Section 4 discusses the wider implications and limitations of the study, with avenues for future research.

2. Methods

2.1. Description of Hybrid Approach to GMSL Rise

The efficient conceptual ESM of *Goodwin* [2016] is used: the Warming Acidification and Sea level Projector (WASP). WASP uses an 8-box representation of the Earth System (see *Goodwin* [2016], Figure 2 therein) and calculates global mean surface warming as a function of cumulative carbon emissions using the equation of *Goodwin et al.* [2015], utilizing additional terms for radiative forcing from non-CO_2 agents [*Goodwin*, 2016; *Williams et al.*, 2016]. Here, the WASP model is extended to incorporate a hybrid approach to simulate GMSL rise. The thermosteric contribution to GMSL rise, $\mathrm{d}(\mathrm{GMSL}_{\mathrm{steric}})/\mathrm{d}t$, is related to the net ocean heat flux, H_{ocean} ($\mathrm{W\,m^{-2}}$), after *Williams et al.* [2012]

$$\frac{\mathrm{d}}{\mathrm{d}t}\left(\mathrm{GMSL}_{\mathrm{steric}}\left(t\right)\right) = c_{\mathrm{steric}} H_{\mathrm{ocean}}\left(t\right) \tag{1}$$

where c_{steric} is the thermosteric sea-level rise per unit ocean heating in $\mathrm{mm\,yr^{-1}}$ $(\mathrm{W\,m^{-2}})^{-1}$. The land-ice volume contribution to GMSL rise, $\mathrm{d}(\mathrm{GMSL}_{\mathrm{ice}})/\mathrm{d}t$, which excludes the land-water storage term, is related to surface warming after *Rahmstorf* [2007]

$$\frac{\mathrm{d}}{\mathrm{d}t}\left(\mathrm{GMSL}_{\mathrm{ice}}\left(t\right)\right) = c_{\mathrm{ice}} \Delta T\left(t\right) \tag{2}$$

where c_{ice} is the semi-empirical coefficient that relates the ice volume component of sea-level rise to global mean surface warming in $\mathrm{mm\,yr^{-1}\,K^{-1}}$ and ΔT is the simulated anthropogenic surface warming since year 1765 in K, where 1765 is the start of the historical forcing scenarios as in *Meinshausen et al.* [2011]. Equations (1) and (2) are combined to give the total GMSL rise excluding land-water storage changes, $\mathrm{d}(\mathrm{GMSL})/\mathrm{d}t$

$$\frac{\mathrm{d}}{\mathrm{d}t}\left(\mathrm{GMSL}\left(t\right)\right) = c_{\mathrm{steric}} H_{\mathrm{ocean}}\left(t\right) + c_{\mathrm{ice}} \Delta T\left(t\right) \tag{3}$$

Equation (3) is used to project GMSL rise in the conceptual ESM to the end of the 21st century, excluding the impacts of changes in land-water storage. Note that this approach is not applied beyond the 21st century

due to the two assumptions inherent in (3), but that do not apply to the longer time-series semi-empirical analysis of *Kopp et al.* [2016]. Firstly, GMSL is assumed to be in static equilibrium at the preindustrial time in (3), and secondly there is no consideration of how c_{ice} may reduce over time as the cryosphere approaches a new equilibrium to elevated global temperatures, which becomes more significant beyond the 21st century [*Orlic and Pasaric*, 2015]. Thus, this study assumes that c_{steric} and c_{ice} remain constant to the end of the 21st century. The impact of these assumptions on the results of this study is revisited in Section 4.

2.2. Constructing Historically Constrained Ensembles

Now we describe how future projections of GMSL are produced using historically constrained ensembles with the conceptual ESM. Future GMSL projections from our new hybrid approach (equation (3)) depend on simulated future warming and ocean heat uptake in the ESM, and on the values of c_{ice} and c_{steric}. To produce an initial ensemble of conceptual ESM simulations, a Monte Carlo approach is adopted with many different combinations of model parameters to generate many different ocean heat uptake and surface warming trajectories.

An initial Monte Carlo ensemble is generated with 10 million conceptual ESM simulations with randomly assigned model parameter values (Figure 2, black). For poorly constrained parameters, random linear input distributions are used covering a wide range of parameter space (Figures 2a–2l, black), and for better-constrained parameters random-normal distributions are employed (Figures 2m–2o, black), where the mean and standard deviations are chosen to approximate the best estimate and uncertainty of these parameters after *Goodwin* [2016].

The simulations are forced with historical CO_2 and radiative forcing from year 1765 to 2005, followed by the IPCC 5th assessment report's four Representative Concentration Pathway (RCP) scenarios after year 2005 [*Meinshausen et al.*, 2011]. Of the four RCP scenarios, RCP3PD (also known as RCP2.6) sees extensive mitigation activities to limit anthropogenic radiative forcing, RCP8.5 is a business as usual case with little mitigation activity, while RCP4.5 and RCP6.0 are intermediate cases [*Meinshausen et al.*, 2011]. From the initial suite of 10 million simulations, three ensembles are extracted based on three different sets of historical constraints, following the methodology of *Goodwin* [2016].

In the initial ensemble of 10 million members, the value of c_{ice} is varied randomly from 0 to 5 mm yr^{-1} K (Figure 2c, black), reflecting the poorly constrained sensitivity of ice volume to increasing global temperatures. The value of c_{steric} is varied with a random-normal distribution, with a mean value of 1.50 mm yr^{-1} (W m^{-2})$^{-1}$ and a standard deviation of 0.30 mm yr^{-1} (W m^{-2})$^{-1}$. Analysis of global mean properties of seawater suggests a thermosteric sea-level rise sensitivity to heating of $c_{steric} = 1.236 \pm 0.116$ mm yr^{-1} (W m^{-2})$^{-1}$ [*Williams et al.*, 2012]. However, this value of c_{steric} assumes uniform ocean heat uptake and uniform seawater properties [*Williams et al.*, 2012]. In reality, anthropogenic ocean heat uptake is systematically biased to upper waters [*Church et al.*, 2011], which have different heat capacity and thermal expansion coefficients than the global whole-ocean mean [*Williams et al.*, 2012; see Figure 1 therein]. Using $c_{steric} = 1.236 \pm 0.116$ mm yr^{-1} (W m^{-2})$^{-1}$ and a net surface heat flux of 0.53 W m^{-2} predicts 0.66 ± 0.05 mm yr^{-1} thermosteric sea-level contribution between 1972 and 2008 [*Williams et al.*, 2012], compared to observations in *Church et al.* [2011] of 0.80 ± 0.15 mm yr^{-1}. Thus, to correct for this discrepancy, the global mean derived value of 1.236 ± 0.116 mm yr^{-1} (W m^{-2})$^{-1}$ is scaled up to $c_{steric} = 1.50 \pm 0.30$ mm yr^{-1} (W m^{-2})$^{-1}$ (Figure 2m, black), such that the coefficient range precisely reproduces the observed trend of 0.80 ± 0.15 mm yr^{-1} sea-level rise from 1972 to 2008 due to a surface heat flux of 0.53 W m^{-2}. This correction to c_{ice} assumes that the systematic bias of anthropogenic heat uptake to particular water masses, leading to the under-estimation from global mean analysis, continues over the next century.

To extract the first ensemble, *SimHist*, constraints are derived from the historical performance of the CMIP5 ensemble in terms of simulated histories of surface warming of the atmosphere and ocean [*Flato et al.*, 2013; *Jha et al.*, 2014; *Song et al.*, 2014], ocean heat uptake [*Flato et al.*, 2013], ocean carbon uptake [*Flato et al.*, 2013], and sea-level rise [*Church et al.*, 2013] (Table 1). Of the initial 10 million ensemble members, the *SimHist* ensemble contains the 94,500 that are consistent with these historic constraints from CMIP5 (Table 1, Figure 2, red). Note that the conceptual ESM used to generate *SimHist*, WASP [*Goodwin*, 2016], is significantly more computationally efficient than the complex models in the CMIP5 ensemble.

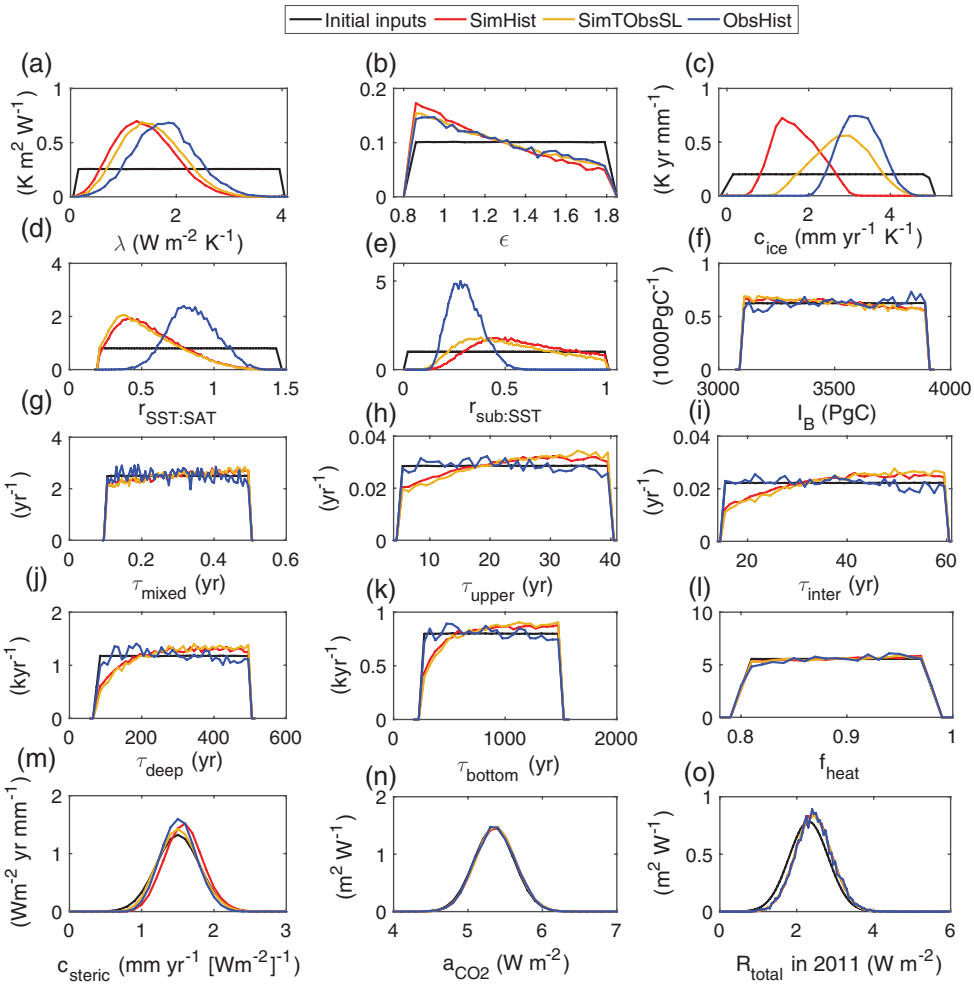

Figure 2. The normalized frequency distributions of model input properties in the Earth system model (ESM) ensembles. Normalized frequency density of the model properties that are varied to produce the initial 10-million member ensemble (black), and then the resulting distributions in the *SimHist* (red), *SimTObsSL* (orange), and *ObsHist* (blue) ensembles. (a) The equilibrium climate parameter, λ (W m^{-2} K^{-1}). (b) The efficacy of ocean heat uptake, ϵ. (c) The coefficient for sea-level rise from ice-melt, c_{ice} (mm K^{-1} yr^{-1}). (d) The ratio of warming for sea surface temperatures to surface air temperatures at equilibrium, $r_{SST:SAT}$. (e) The ratio of sub-surface ocean warming to sea surface temperature warming at equilibrium, $r_{sub:SST}$. (f) The buffered carbon inventory of the atmosphere–ocean system, I_B (PgC). (g) The e-folding timescale for the surface mixed layer dissolved inorganic carbon (DIC) to equilibrate relative to a fixed atmospheric CO_2 concentration, τ_{mixed} (yr). (h)–(k) The e-folding timescales for sub-surface ocean tracers to equilibrate relative to a fixed mixed layer value: τ_{upper} (yr) for the upper ocean region, τ_{inter} (yr) for the intermediate ocean region, τ_{deep} (yr) for the deep ocean region, and τ_{bottom} (yr) for the bottom ocean region. (l) The fraction of total Earth system heat uptake in the ocean, f_{heat}. (m) The coefficient for sea-level rise from thermal expansion, c_{steric} (mm yr^{-1} [W m^{-2}]$^{-1}$). (n) The radiative forcing from a log-change in atmospheric CO_2, a_{CO2} (W m^{-2}). (o) The total radiative forcing from all agents in 2011, R_{total} (W m^{-2}). For a full definition of each term in the ESM see *Goodwin* [2016].

In the second ensemble, *SimTObsSL*, some of the constraints are derived from CMIP5 simulated histories and the other constraints are derived from historic observations. For surface warming, ocean heat uptake and ocean carbon uptake, the constraints for *SimTObsSL* are derived from the CMIP5 historic simulations, and so match the constraints for *SimHist* (compare Table 2 to Table 1). However, for total and thermosteric sea-level rise, the constraints used to extract the *SimTObsSL* ensemble are taken from historic observations [*Church et al.*, 2013] (Table 2). Note that the historic constraint for total observed sea-level rise from 1901 to 1990 (Table 2) has had the land-water storage component [*Church et al.*, 2013] removed, as this component is not simulated in equation (3). The *SimTObsSL* ensemble contains 63,600 members, from the initial 10 million, that are consistent with the historic constraints used (Table 2, Figure 2, orange).

The final ensemble, *ObsHist*, is extracted from the initial 10 million simulations using constraints entirely derived from historic observations (Table 3). The *ObsHist* constraints are derived from observations of

Table 1. The Historical Constraints for the *SimHist* Ensemble

Climate System Property	Historic Constraint From CMIP5 Simulations	*SimHist* Range
Warming from 1850 to 1961–1990 average	0.1–1.0 K [*Song et al.*, 2014]	0.26–1.0 K
Warming from 1961–1990 average to 2005	0.3–1.1 K [*Song et al.*, 2014]	0.3–0.95 K
Decadal warming rate from 1951 to 2012	0.05–0.23 K decade^{-1} [*Flato et al.*, 2013]	0.06–0.23 K decade^{-1}
SST increase 1870–1900 to 1986–2005	0.2–0.7 K [*Jha et al.*, 2014]	0.2–0.7 K
Whole-ocean heat content increase from 1971 to 2005	80–380 ZJ [*Flato et al.*, 2013]	112–380 ZJ
Upper 700 m ocean heat content increase from 1971 to 2010	25–370 ZJ [*Flato et al.*, 2013]	50–224 ZJ
Ocean carbon uptake from 1986 to 2005	1.6–2.3 PgC yr^{-1} [*Flato et al.*, 2013]	1.6–2.3 PgC yr^{-1}
Ice volume contribution to GMSL rise from 1901 to 1990 (excluding land-water storage)	0.42–0.98 mm yr^{-1} [*Church et al.*, 2013]	0.42–0.98 mm yr^{-1}
Thermosteric contribution to GMSL rise, 1993–2010	0.97–2.02 mm yr^{-1} [*Church et al.*, 2013]	0.97–2.02 mm yr^{-1}

CMIP5, Climate Model Intercomparison Project phase 5; GMSL, global mean sea level; SST, sea surface temperature. All historic constraints are taken from the performance of the CMIP5 simulations, as analyzed in *Song et al.* [2014], *Flato et al.* [2013], *Jha et al.* [2014], and *Church et al*. [2013]. To be consistent with the tests, a *SimHist* ensemble member must satisfy all constraints.

historic surface warming [*Hartmann et al.*, 2013; *Rhein et al.*, 2013], ocean heat uptake [*Rhein et al.*, 2013], ocean carbon uptake [*Ciais et al.*, 2013], and sea-level rise [*Church et al.*, 2013]. Again, the land-water storage component of total observed historic sea-level rise from 1901 to 1990 is removed from the *ObsHist* constraint (Table 3). *ObsHist* contains 12,800 ensemble members that are consistent with the historic observational constraints (Table 3, Figure 2, blue).

The land-water storage component of total historic sea-level rise is removed from the observational constraints (Tables 2 and 3) as follows. First, it is assumed that the 90% ranges in the historical observations for GMSL from 1901 to 1990 in *Church et al.* [2013] reflect normal uncertainty distributions, both for the ranges of total GMSL rise and the component contributions from different processes. The historic land-water storage component is then extracted from the total sea-level rise (assuming that the uncertainties in each are independent and combine in quadrature according to the standard rules for normally distributed uncertainty propagation) to construct the total GMSL rise excluding land-water storage (Tables 2 and 3).

To generate future projections, future land-water storage changes must be incorporated in all three ensembles, *SimHist*, *SimTObsSL*, and *ObsHist*, and added to the GMSL rise calculated using (3). The future land-water storage contributions are assumed to increase GMSL from 1986–2005 to 2081–2100 by between −0.01 and +0.09 m after *Church et al.* [2013]. For each conceptual ESM ensemble member, a random linear land-water storage future sea-level contribution is assigned between these limits.

2.3. Calculating the Change in Frequency of Extreme Sea Level Events

Prior to estimating the likely increase in frequency of extreme sea levels, we account for variations in regional sea-level rise at each of the 220 sites, using the regional patterns from *Slangen et al.* [2014]. Using a combination of model results and observations, *Slangen et al.* [2014] produced regional projections of sea level that separately account for spatial variations resulting from ocean circulation, increased heat uptake, atmospheric pressure, regional contributions of land ice (glaciers and ice sheets), groundwater depletion, and glacial isostatic adjustment, including gravitational effects due to mass redistribution. We superimposed the ensemble-mean regional patterns of each of their individual components [see *Slangen et al.*, 2014, Figure 1

Table 2. The Historic Constraints for the SimTObsSL Ensemble

Climate System Property	Historic Constraint From CMIP5 or Observations	SimTObsSL Range
Warming from 1850 to 1961–1990 average	0.1–1.0 K [*Song et al.*, 2014]	0.25–1.0 K
Warming from 1961–1990 average to 2005	0.3–1.1 K [*Song et al.*, 2014]	0.3–0.91 K
Decadal warming rate from 1951 to 2012	0.05–0.23 K decade^{-1} [*Flato et al.*, 2013]	0.06–0.23 K decade^{-1}
SST increase 1870–1900 to 1986–2005	0.2–0.7 K [*Jha et al.*, 2014]	0.2–0.7 K
Whole-ocean heat content increase from 1971 to 2005	80–380 ZJ [*Flato et al.*, 2013]	102–380 ZJ
Upper 700 m ocean heat content increase from 1971 to 2010	25–370 ZJ [*Flato et al.*, 2013]	49–219 ZJ
Ocean carbon uptake from 1986 to 2005	1.6–2.3 PgC yr^{-1} [*Flato et al.*, 2013]	1.6–2.3 PgC yr^{-1}
Total GMSL rise from 1901 to 1990 (from historic observations, excluding land-water storage)	1.4–1.8 mm yr^{-1} [*Church et al.*, 2013]	1.4–1.8 mm yr^{-1}
Thermosteric contribution to GMSL rise, 1993–2010	0.8–1.4 mm yr^{-1} [*Church et al.*, 2013]	0.8–1.4 mm yr^{-1}

CMIP5, Climate Model Intercomparison Project phase 5; GMSL, global mean sea level; SST, XXX.
Historic constraints for sea-level rise taken from observations [*Church et al.*, 2013], all other historic constraints taken from the performance of the CMIP5 simulations, as analyzed in *Song et al.* [2014] and *Flato et al.* [2013]. To be consistent with the tests, a *SimTObsSL* ensemble member must satisfy all constraints.

therein] onto our GMSL projections, to estimate the corresponding relative sea-level rise projections at the 220 tide-gauge sites we consider (see below). This was achieved by removing the global mean value from the *Slangen et al.* [2014] regional analysis. Note, while these relative sea-level rise projections account for regional vertical land movement at each site, resulting from glacial isostatic adjustment, they do not account for localized vertical land movement arising from processes like tectonics or subsidence due to groundwater extraction, which can be large at certain locations (e.g., Bangkok; *Nicholls* [1995]).

To estimate the likely increase in frequency of extreme sea-level events, we use hourly sea-level records (of at least 30 years in length) at 220 sites, from an updated version of the Global Extreme Sea Level Analysis (http://www.gesla.org) tide-gauge dataset [see *Mawdsley et al.*, 2015 for details]. The names and locations of these 220 sites, and the length of the available records are each, are listed in *Mawdsley et al.* [2015], Table S1 therein. At each site, we fit a generalized extreme-value (GEV) distribution to time-series of annual maximum sea level (declustered to ensure they correspond to unique events), to estimate the GEV scale parameter (λ_{GEV}). Following the approach of *Hunter* [2012], we then estimated, for the range of GMSL-rise projections considered above, the factor increase in the expected number of sea-level exceedances (N) by calculating $N = \exp(\delta z/\lambda_{GEV})$, where δz is a rise of GMSL. Note that this only accounts for the direct effect of a rise in mean sea level, which results in a lower storm-surge elevation at high tide being necessary to produce a sea level high enough to cause flooding; it does not account for indirect effects (i.e., changes in water depth altering tidal propagation or surge generation) or changes arising from future variations in the frequency, intensity or tracks of storms.

3. Results

Our future GMSL projections, made relative to the average GMSL during the 1986–2005 period, are presented in Section 3.1, while the projected changes in frequency of extreme sea-level events at 220 coastal cities are presented in Section 3.2.

Table 3. The Historical Constraints for the *ObsHist* Ensemble

Historic Ocean Heat and Carbon Property	Observation Constraint (90% Range)	*ObsHist* (5th to 95th Percentile)
Decadal SST warming from 1971 to 2010	0.09–0.13 K decade^{-1} [*Rhein et al.*, 2013]	0.08–0.13 K decade^{-1}
Earth system heat content increase, 1971–2010	196–351 ZJ [*Rhein et al.*, 2013]	238–360 ZJ
Earth system heat content increase, 1993–2010	127–201 ZJ [*Rhein et al.*, 2013]	119–183 ZJ
Upper 700 m ocean heat content increase, 1971–2010	82–164 TW [*Rhein et al.*, 2013]	93–138 TW
Cumulative ocean carbon uptake	125–185 PgC [*Ciais et al.*, 2013]	123–174 PgC
Warming from 1850–1900 to 1993–2012	0.72–0.85 K [*Hartmann et al.*, 2013]	0.70–0.85 K
Decadal warming rate from 1951 to 2012	0.09–0.14 K decade^{-1} [*Hartmann et al.*, 2013]	0.09–0.11 K decade^{-1}
Total GMSL rise from 1901 to 1990 (from observations, excluding land-water storage)	1.4–1.8 mm yr^{-1} [*Church et al.*, 2013]	1.4–1.8 mm yr^{-1}
Thermosteric contribution to GMSL rise, 1993–2010	0.8–1.4 mm yr^{-1} [*Church et al.*, 2013]	0.8–1.4 mm yr^{-1}

GMSL, global mean sea level; SST, XXX.
All historic constraints are taken from observations after *Rhein et al.* [2013], *Ciais et al.* [2013], *Hartmann et al.* [2013], and *Church et al.* [2013]. An *ObsHist* ensemble member is considered observationally consistent if it satisfies at least eight of the nine observational 90%-range constraints. If it satisfies only eight constraints within the 90% range, then it must be within an extra 50% of the remaining observational constraint's range. This allows the tails of the observational constraints to be included within the *ObsHist* ensemble, and follows the methodology of *Goodwin* [2016].

3.1. Projections of GMSL Rise for RCP Scenarios

The projection ranges of surface warming in *SimHist*, relative to the 1986–2005 average, are similar to the CMIP5 projections for each RCP scenario over the 21st century (Figure 1a, compare red to black) because the historical performance ranges of CMIP5 are used as constraints to identify the ensemble members for the *SimHist* ensemble from our efficient conceptual ESM [*Goodwin*, 2016] (Table 1). Given this similarity in both historical and future warming (Table 1, Figure 1a), we can directly compare the mechanistic future sea-level projection ranges from CMIP5 with our hybrid approach sea-level ranges in the *SimHist* ensemble.

The future hybrid sea-level-projection ranges in *SimHist* closely match the future process-based projection ranges from the CMIP5 ensemble across the 21st century, both for total GMSL (Figure 1b, compare red to black) and for the thermosteric component (Figure 1c, compare red to black). The historical warming and sea-level constraints from the CMIP5 ensemble constrain the ice-melt sensitivity to warming to $c_{ice} = 1.7 \pm 0.5$ mm yr^{-1} K^{-1} in the *SimHist* ensemble (Figure 2c, red). Applying this range of c_{ice} into the future in *SimHist* reproduces the CMIP5-ensemble GMSL ranges (Figure 1b, compare red to black), and results in an ensemble-mean projection of GMSL rise in *SimHist* over the 21st century that is within ±2 cm of the CMIP5 ensemble mean for each RCP scenario (Figure 1b).

Thus, we have shown that the CMIP5 process-based simulations of GMSL from the start of the 20th century (Table 1) to the end of the 21st century (Figure 1), for the given temperature evolution ranges (Figure 1a, Table 1), are consistent with a constant ice-melt-related GMSL sensitivity to warming over time, of $c_{ice} = 1.7 \pm 0.5$ mm yr^{-1} K^{-1} (Figure 2c, red). While this constant-in-time linear sensitivity (equation (3)) may not hold for any particular ice-melt process or CMIP5 model [*Church et al.*, 2013], the constant linear ice-melt sensitivity of 1.7 ± 0.5 mm yr^{-1} K^{-1} over the 20th and 21st centuries does encapsulate the CMIP5 ensemble projection-range as a whole, which comprises the aggregation of responses of all ice-melt processes within all models in all CMIP5 ensemble members (Figure 1, Table 1).

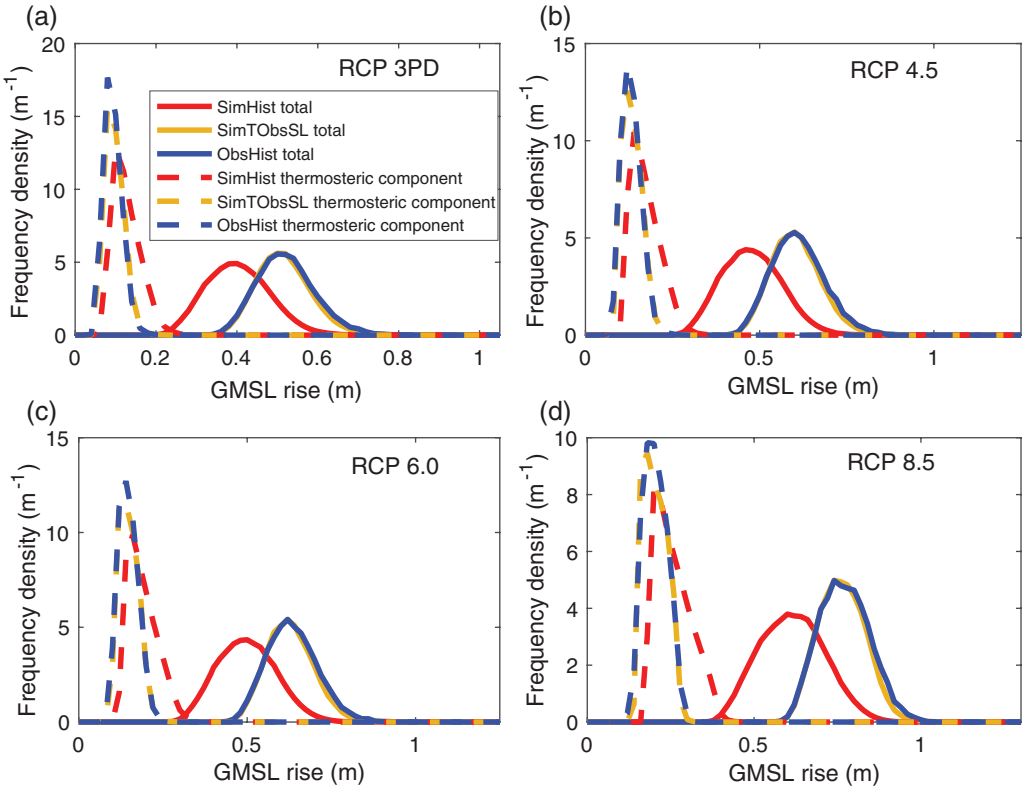

Figure 3. Normalized frequency distributions of future global mean sea level (GMSL) rise from 1986–2005 to 2081–2100 in three model ensembles for Representative Concentration Pathway (RCP) scenarios. Shown are the projections for total GMSL rise (solid lines) and the thermosteric contribution (dashed lines).

A question might be posed whether the CMIP5 process-based projections (Figure 1, black) are superior to the hybrid approach (3) due to their explicitly modeled nonlinear ice-melt behavior. However, here this issue is refocused to ask—given that $c_{ice} = 1.7 \pm 0.5$ mm yr^{-1} K^{-1} fully encapsulates the CMIP5 process-based projection ranges (Figure 1b, red and black)—whether this effective ice-melt sensitivity range in the process-based projections is actually a good estimate for the real-world sensitivity over the 20th and 21st centuries?

The second model ensemble, *SimTObsSL*, contains 63,600 members that are consistent with historical CMIP5 surface warming, and also consistent with historical observations for thermosteric and total GMSL rise (Table 2). Again historical and future warming, relative to the 1986–2005 average, is consistent with CMIP5 across the 20th and 21st centuries (Table 2, Figure 1a, compare orange to black). However, to be consistent with historical GMSL observations (Table 2), the range of ice-melt sensitivity to warming in *SimTObsSL* is increased to $c_{ice} = 2.8 \pm 0.7$ mm yr^{-1} K^{-1} (Figure 2c, orange). This increase indicates that the upper bounds of ice-melt sensitivity to warming consistent with historical GMSL observations (Figure 2c, orange) are present neither in the *SimHist* ensemble (Figure 2c, red), nor in the process-based CMIP5 ensemble. This observational constraint to c_{ice} yields future projections of total GMSL rise in *SimTObsSL* (Figure 3, orange) that exceed the CMIP5 projections (Figure 1b, compare orange to black; Table 4); the mean GMSL projections for the 2081–2100 period in *SimTObsSL* exceed CMIP5 by between 13 and 16 cm for the four RCP scenarios.

In the third ensemble, *ObsHist* ($n = 12{,}800$, Section 2.2, Table 3), the future warming projections have a similar lower bound, but a reduced upper bound, relative to CMIP5 (Figure 1a, compare blue to black). This discrepancy results from differences in the historical constraints derived from observations, relative to those derived from the CMIP5 performance (Tables 1–3), most notably for historical warming [*Goodwin*, 2016].

Despite its reduced future warming and reduced thermosteric contributions to sea-level rise (Figures 1a and 1c, compare blue with black), the *ObsHist* ensemble still gives GMSL projections relative to 1986–2005 consistent with *SimTObsSL* (Figure 1, blue, orange), and increased relative to those from CMIP5 (Figure 1b,

Table 4. GMSL Rise Relative to 1986–2005 Average in the Conceptual ESM Ensembles

Model ensemble	RCP3PD	RCP4.5	RCP6.0	RCP8.5
	GMSL rise at 2100 from 1986 to 2005 average (*mean* [*5th to 95th percentile*] in cm)			
SimHist	44 [31–59]	53 [38–70]	57 [41–74]	72 [53–91]
SimTObsSL	57 [45–70]	68 [55–82]	72 [59–86]	89 [76–103]
ObsHist	57 [45–72]	69 [55–84]	73 [59–88]	90 [76–105]
	GMSL rise at 2100 from 1986 to 2005 average (*99th percentile* in cm)			
SimHist	66	78	82	98
SimTObsSL	77	90	94	110
ObsHist	79	92	96	112
	GMSL rise at 2081–2100 average from 1986 to 2005 average (*mean* [*5th to 95th percentile*] in cm)			
SimHist	40 [28–53]	48 [34–62]	50 [36–65]	61 [46–78]
SimTObsSL	52 [41–63]	60 [49–73]	63 [52–75]	76 [65–88]
ObsHist	52 [41–65]	61 [49–75]	63 [52–76]	77 [65–90]

CMIP5, Climate Model Intercomparison Project phase 5; ESM, Earth system model; GMSL, global mean sea level. The mean, 5th and 95th percentiles of GMSL rise by 2100 and for the 2081–2100 average in the *SimHist* ensemble are comparable to the equivalent figures for the CMIP5 ensemble [see *Church et al.*, 2013; Table 13.5 therein]: for each scenario the *SimHist* ensemble-mean GMSL rise is within 2 cm of the CMIP5 ensemble-mean for both 2100 and 2081–2100 periods. Greater GMSL rise is observed in the *SimTObsSL* and *ObsHist* ensembles. The large number of ensemble members in the *SimHist*, *SimTObsSL*, and *ObsHist* ensembles allows the 99th percentile GMSL rise to be identified.

compare blue to black) and *SimHist* (Figures 1b, and 3, compare blue to red). *ObsHist*'s exclusive use of historical observations to constrain c_{ice} and the ESM (Tables 3) gives $c_{ice} = 3.2 \pm 0.5$ mm yr^{-1} K^{-1} (Figure 2c, blue). This is a higher mean and a narrower range than in *SimTObsSL*, which instead uses CMIP5-simulations to constrain historical warming (Figure 2c, compare blue to orange).

The similarity in future sea-level rise projections between the *ObsHist* and *SimTObsSL* ensembles is understood by comparing the distributions of model parameter values (Figure 2, compare blue to orange). The equilibrium climate parameter, λ (W m^{-2} K^{-1}) (Figure 2a), strongly affects future warming: higher values of λ generally lead to lower values of future warming for a given radiative forcing [e.g., *Goodwin*, 2016; *Goodwin et al.*, 2015]. This reduced future warming in turn leads to relatively reduced ice-melt and lower future GMSL rise. The value of c_{ice} (Figure 2c) strongly affects future GMSL rise: higher values of c_{ice} lead to higher ice-melt contribution to GMSL rise for a given future warming. Thus, all else being equal, higher values of λ lead to lower future GMSL rise from reduced warming, while higher values of c_{ice} lead to higher future GMSL rise from increased sensitivity of ice-melt to warming.

The *ObsHist* and *SimTObsSL* ensembles achieve the same historic total GMSL rise from 1901 to 1990 (Tables 2 and 3) due to the opposing effects of higher c_{ice} values and higher λ values in *ObsHist* compared to *SimTObsSL* (Figures 2a and 2c, compare blue to orange). These opposing effects of higher values of both λ and c_{ice} in *ObsHist* also result in very similar GMSL rise projections in the future (Figures 1 and 3, compare blue to orange). In contrast, the *SimHist* ensemble projects less future GMSL rise than *SimTObsSL*, because *SimHist* has similar values of λ (Figure 2a, compare red to orange) but significantly lower values of c_{ice} (Figure 2c, compare red to orange).

3.2. Projections of the Change in Frequency of Extreme Sea Level Events

The factor increase in expected frequency of extreme sea level events describes the decrease in expected return period. For example, an extreme sea level event that is expected to occur once every 100 years would, following a 100 factor increase, be expected to occur once every year. Any future rise in GMSL increases the expected frequency of hazardous extreme sea-level events [*McGranahan et al.*, 2007]. Illustrated for New York and Manila, our higher GMSL projections by 2100 of *SimTObsSL* and *ObsHist* (Table 4), which use real-world observations to constrain c_{ice}, lead to a strong increase in expected frequency of extreme sea-level events, relative to the CMIP5 or *SimHist* ensemble projections (see Figures 4a–4d). At Manila, which has a flatter return period curve, water levels that are currently only exceeded during very low probability

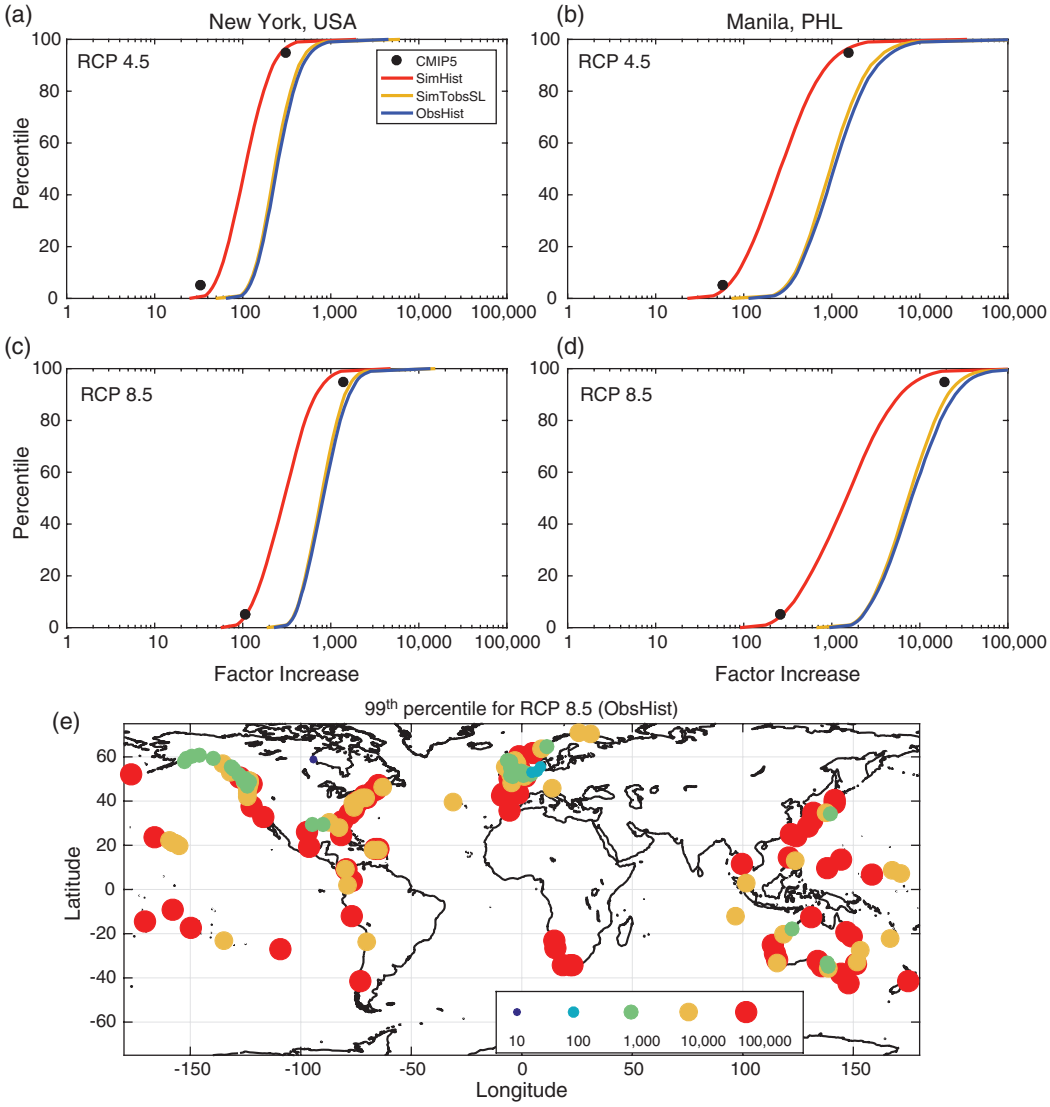

Figure 4. Factor increase in the frequency of extreme sea level events at 2100 relative to 1986–2005 period. The factor increase in extreme sea level events for Representative Concentration Pathway (RCP4.5) at (a) New York and (b) Manila, and for RCP8.5 at (c) New York and (d) Manila; for the 5th and 95th percentiles of CMIP5 (black dots) and the SimHist (red line), SimTObsSL (orange line) and ObsHist (blue line) ensemble projections. (e) The factor increase in frequency of extreme sea level events at 220 cites worldwide for the 99th percentile projection in the *ObsHist* ensemble.

storm-surge events (i.e., in 100 year return levels or higher) are likely to be exceeded virtually every high water by 2100 for the RCP8.5 scenario, under just normal tidal conditions. This corresponds to a >10,000 factor increase in the frequency of extreme sea-level events at this site for the upper percentiles (>~60th percentile) of our projected distribution. At New York, which has a steeper return period curve, water levels that are currently only exceeded during very low-probability storm-surge events (i.e., in 100-year return levels or higher) are likely to be exceeded several times a year by 2100 for the RCP8.5 scenario, under smaller storm conditions. This corresponds to a >1,000 factor increase in the frequency of extreme sea-level events at this site for the upper percentiles (>~70th percentile) of our projected distribution.

This has obvious implications for the frequency of extreme sea-level events that may be expected in coastal cities around the world, as is illustrated in Figure 4e for the business as usual emissions scenario RCP 8.5. At most tide-gauge sites around the world there is at least a factor 1,000 increase in the frequency of extreme sea-level events by 2100. This impacts on coastal conservation, adaptation, and defence, infrastructure planning and management, and emergency response planning.

The highly resolved frequency distributions (Figure 3) of our hybrid approach results, across a wide parameter space, are exploited to better explore the low-frequency, high-impact upper tail of the sea-level projections (Figure 4; Table 4). Even for the RCP scenario with strongest mitigation (RCP3PD/RCP2.6), the 99th percentile of GMSL rise reaches at least 66 cm.

4. Discussion and Implications

The analysis presented here shows that the GMSL projection ranges from the CMIP5-based suite of process-based models [*Church et al.*, 2013, *Slangen et al.*, 2014] are consistent with a constant ice-melt sensitivity over the 20th and 21st centuries of 1.7 ± 0.5 mm yr^{-1} K^{-1} (Figure 1, compare black and red; Figure 2c, red). However, this does not include the full range consistent with historical observations (Table 3), which increases the sensitivity up to 3.2 ± 0.5 mm yr^{-1} K^{-1} (Figure 2c, blue). When the observational adjustments to the ice-melt sensitivity are applied, this indicates that CMIP5-based GMSL projections for the year 2100 should be revised upwards by between 13 and 16 cm across the RCP scenarios (Table 4, Figure 1, compare orange and blue to black).

One limitation in our hybrid sea-level approach (equation (3)) is that there may be large nonlinearities in the sensitivity of different parts of the cryosphere to warming, for example, due to historically unprecedented processes [*deConto and Pollard*, 2016], which cannot be captured by the constant c_{ice}. This limitation is a general issue in many semi-empirical GMSL methods, but can be addressed within process-based methods [*Church et al.*, 2013]. However, note that while any single CMIP5 projection may include significant nonlinearities from the resolved processes, as a whole the CMIP5 ensemble GMSL simulated ranges are entirely consistent with the constant linear cryosphere response to warming of $c_{ice} = 1.7 \pm 0.5$ mm yr^{-1} K^{-1} of the *SimHist* ensemble (Figure 2c, red), both for the 20th (Table 1) and 21st (Figure 1, compare red to black) centuries.

Unlike the computationally expensive CMIP5 ensemble projections [*Church et al.*, 2013], the computational efficiency of our method allows frequency density distributions for the future GMSL rise projections to be produced (Figure 3). Previous studies have produced probability density distributions for future GMSL rise projections, for example, *Kopp et al.* [2014], *Jevrejeva et al.* [2014] and *Grinsted et al.* [2015]. However, all three of these studies utilized, to some degree, both expert elicitation [*Bamber and Aspinall*, 2013] and the existing CMIP5-derived AR5 future GMSL projections [*Church et al.*, 2013] in their methodologies (along with other considerations). In contrast, the *SimHist*, *SimTObsSL*, and *ObsHist* projections presented here (Figure 3) contain neither expert elicitation nor the future projections of the CMIP5 ensemble. Indeed, the *ObsHist* ensemble projections (Figure 3, blue) do not contain information from the historic performance of the CMIP5 models either, but instead are constrained entirely by historic observations (Table 3). Thus, the frequency density projections produced here (Figure 3) represent probability distributions under the assumption that the sensitivity of the cryosphere to temperature in the 21st century remains identical to that of the 20th century. Note that the upper bounds of projected sea-level rise (Figures 1 and 3, Table 4) may still underestimate the uppermost extreme possibilities, as our historical-observation-based method cannot capture historically unprecedented processes [e.g., *deConto and Pollard*, 2016] that might arise from the exceptional anthropogenic forcing of climate. Regardless, our upper bounds present useful and realistic planning targets, when viewed alongside continued environmental monitoring for early detection of superimposed, historically unprecedented processes. Such high-end sea-level scenarios play an important role in the planning of coastal risk-management, such as the Thames Estuary 2100 project for London [*Hinkel et al.*, 2015].

We now consider two further limitations in our hybrid approach. The hybrid approach assumes a static (equilibrium) starting point for GMSL at preindustrial times, and that there is no adjustment in c_{ice} over time as cryosphere system adjusts towards a new equilibrium at elevated global temperatures. To address these issues would require longer timescale simulation starting at the Last Glacial Maximum. This is because there is no way to constrain the timescales over which c_{ice} should be adjusted over time, or the extent to which the cryosphere was out of equilibrium at preindustrial times, using the historical constraint method (Table 3) without performing simulations over longer timescales. It should be noted, when comparing the *SimHist* ensemble to the CMIP5 projections, that neither the *SimHist* nor CMIP5 ensembles explicitly simulate the most recent deglaciation, and that the GMSL projection ranges agree both historically (Table 1) and for the

future (Figure 1) without adjusting c_{ice} in the *SimHist* ensemble over time. Thus, neither of these assumptions significantly affects the results of the *SimHist* ensemble when comparing the hybrid approach (equation (3)) to CMIP5. However, for the *SimTObsSL* and *ObsHist* ensembles, where historical sea-level constraints arise from observations (Tables 2 and 3), any cryospheric adjustment to GMSL from the last deglaciation occurring between 1901 and 1990 should be removed from the historical tests. *Lambeck et al.* [2014] noted that sea level was essentially stable over the past 6,000 years, which suggests that such corrections are small even if necessary. Further research is needed to evaluate this in more detail.

In the hybrid approach used here, the coefficient c_{ice} (equations (2) and (3)) represents the GMSL response of the entire cryosphere to rising temperatures. Separating the individual components of the cryosphere (e.g., glaciers, the Greenland ice sheet and the Antarctic ice sheets) is beyond the scope of this study since, again, longer timescale constraints would have to be applied to separate the different timescales of each component. However, it should be noted that the thermal expansion and ice-sheet components of GMSL rise are separated (Figures 1 and 3), and that this separation in the *SimHist* ensemble agrees with the CMIP5 ensemble (Figure 1, compare red to black).

Finally, we infer that WASP is a conceptual ESM that is capable of producing 21st century global mean warming (Figure 1a) and GMSL projections (Figures 1b, 1c, and 3) that are similar to the CMIP5 projection ranges for all four RCP scenarios (Figure 1, compare red to black), but at greatly reduced computational cost. The WASP model can generate approximately 1000 ensemble members per Central Processing Unit (CPU) second on a standard desktop computer, each simulating from year 1765 to 2100. This low computational cost means that WASP can quickly produce projections for other, arbitrary, future scenarios. In addition, WASP could be used for projecting out much further (e.g., 2300) to assess, for example, the long-term commitment to sea-level rise [e.g., *Foster and Rohling* 2013; *Levermann et al*., 2013; *Rohling et al*., 2013]. This computational efficiency makes the GMSL and warming projections of WASP potentially useful for purposes such as a relative impact analysis of alternative scenarios, or for inclusion within an Integrated Assessment Modelling framework.

5. Conclusions

Our hybrid approach to GMSL projections gives similar results to the IPCC AR5 projections (Figure 1) [*Church et al*., 2013] when historic CMIP5 simulations are used to constrain the methodology (Table 1). However, historic sea-level rise is better quantified by direct observations than by simulations. When historic observations are used to constrain the hybrid approach (Tables 2 and 3), we project an additional 13–16 cm more GMSL rise by the end of the 21st century than the IPCC AR5 simulations (Figures 1 and 3; Table 4). This additional GMSL rise then leads to a larger reduction in the return time for extreme sea level events (Figures 4a–4d). The large ensemble-size of our methodology also allows full frequency density projections to be produced (Figure 3), and the high-impact low-probability tails of future GMSL rise to be investigated (Figure 4e).

Coastal planning and adaptation measures for the 21st century should take into account both the additional GMSL rise projected using observational constraints, and the additional increase in the frequency of local extreme sea level events that this causes, and the high-impact low-probability projections our method produces.

Acknowledgments
This work was supported by a UK Natural Environment Research Council (NERC) grants NE/P01495X/1 and NE/N009789/1, and contributes to UK-NERC consortium iGlass (NE/I009906/1). EJR acknowledges support from Australian Laureate Fellowship FL120100050.

References

Bamber, J. L., and W. P. Aspinall (2013), An expert judgement assessment of future sea level rise from the ice sheets, *Nat. Clim. Change*, *3*, 424–427, doi:10.1038/nclimate1778.

Ciais, P., et al (2013), Carbon and other biogeochemical cycles, in *Climate Change 2013: The Physical Science Basis*, edited by T. F. Stocker et al , pp. 465–570 , IPCC, Cambridge Univ. Press, Cambridge, U. K. and New York, N. Y.

Collins, M., et al. (2013), Long-term climate change: Projections, commitments and irreversibility, in *Climate Change 2013: The Physical Science Basis*, edited by T. F. Stocker et al. , pp. 1029–1136 , IPCC, Cambridge Univ. Press, Cambridge, U. K. and New York, N. Y.

Church, J. A., et al. (2011), Revisiting the Earth's sea-level and energy budgets from 1961 to 2008, *Geophys. Res. Lett.*, *38*, L18601, doi:10.1029/2011GL048794.

Church, J. A., et al. (2013), Sea level change, in *Climate Change 2013: The Physical Science Basis*, edited by T. F. Stocker et al. , pp. 1137–1216, IPCC, Cambridge Univ. Press, Cambridge U. K. and New York, N. Y.

deConto, R. M., and D. Pollard (2016), Contribution of Antarctica to past and future sea-level rise, *Nature*, *531*, 591–597, doi:10.1038/nature17145.

Flato, G., et al (2013), Evaluation of climate models, in *Climate Change 2013: The Physical Science Basis*, edited by T. F. Stocker et al. , pp. 741–866 , IPCC, Cambridge Univ. Press, Cambridge, U. K. and New York, N. Y.

Foster, G.L., and Rohling, E.J. (2013). Relationship between sea level and climate forcing by CO_2 on geological timescales. *Proc. Natl. Acad. Sci. U. S. A., 110*, 1209–1214, 2013.
Goodwin, P. (2016), How historic simulation-observation discrepancy affects future warming projections in a very large model ensemble, *Clim. Dyn.*, *47*(7), 2219–2233, doi:10.1007/s00382-015-2960-z.
Goodwin, P., R. G. Williams, and A. Ridgwell (2015), Sensitivity of climate to cumulative carbon emissions due to compensation of ocean heat and carbon uptake, *Nat. Geosci.*, *8*, 29–34, doi:10.1038/ngeo2304.
Grinsted, A., S. Jevrejeva, R. E. M. Riva, and D. Dahl-Jensen (2015), Sea level projections for northern Europe under RCP8.5, *Clim. Res.*, *64*, 15–33, doi:10.3354/cr01309.
Hartmann, D. L., et al (2013), Observations: Atmosphere and surface, in *Climate Change 2013: The Physical Science Basis*, edited by T. F. Stocker et al., pp. 159–254 , IPCC, Cambridge Univ. Press, Cambridge, U. K. and New York, N. Y.
Hinkel, J., et al. (2015), Sea-level rise scenarios and coastal risk management, *Nat. Clim. Change*, *5*, 188–190, doi:10.1038/nclimate2505.
Hunter, J. (2012), A simple technique for estimating an allowance for uncertain sea-level rise, *Clim. Change*, *113*, 239–252, doi:10.1007/s10584-011-0332-1.
Jevrejeva, S., J. C. Moore, and A. Grinsted (2012), Sea level projections to AD 2500 with a new generation of climate change scenarios, *Global Planet. Change*, *80–81*, 14–20, doi:10.1016/j.gloplacha.2011.09.006.
Jevrejeva, S., A. Grinsted, and J. C. Moore (2014), Upper limit for sea level projections by 2100, *Environ. Res. Lett.*, *9*, 1–9, doi:10.1088/1748-9326/9/10/104008.
Jha, B., Z.-Z. Hu, and A. Kunar (2014), SST and ENSO variability and change simulated in historical experiments of CMIP5 models, *Clim. Dyn.*, *42*, 2113–2124, doi:10.1007/s00382-013-1803-z.
Kopp, R. E., et al (2016), Temperature-driven global sea-level variability in the Common Era, *Proc. Natl. Acad. Sci. U. S. A.*, *113*(11), 1434–1441, doi:10.1073/pnas.1517056113.
Kopp, R. E., R. M. Horton, C. M. Little, J. X. Mitrovica, M. Oppenheimer, D. J. Rasmussen, B. H. Strauss, and C. Tebaldi (2014), Probabilistic 21st and 22nd century sea-level projections at a global network of tide-gauge sites, *Earth's Future*, *2*, 383–406, doi:10.1002/2014EF000239.
Lambeck, K., et al. (2014), Sea level and global ice volumes from the Last Glacial Maximum to the Holocene, *Proc. Natl. Acad. Sci.U. S. A.*, *111*(43), 15296–15303, doi:10.1073/pnas.1411762111.
Levermann, A., et al. (2013), The multimillennial sea-level commitment of global warming, *Proc. Natl. Acad. Sci.U. S. A.*, *110*(34), 13745–13750, doi:10.1073/pnas.1219414110.
Marzeion, B., A. H. Jarosch, and M. Hofer (2012), Past and future sea-level changes from the surface mass balance of glaciers, *Cryosphere*, *6*, 1295–1322, doi:10.5194/tc-6-1295-2012.
Mawdsley, R. J., I. D. Haigh, and N. C. Wells (2015), Global secular changes in different tidal high water, low water and range levels, *Earth's Future*, *3*(2), 66–81, doi:10.1002/2014EF000282.
McGranahan, G., D. Balk, and B. Anderson (2007), The rising tide: Assessing the risks of climate change and human settlements in low elevation coastal zones, *Environ. Urban.*, *19*, 17–37, doi:10.1177/0956247807076960.
Meinshausen, M., et al. (2011), The RCP greenhouse gas concentrations and their extensions from 1765 to 2300, *Clim. Change*, *109*, 213–241, doi:10.1007/s10584-011-0156-z.
Nicholls, R. J. (1995), Coastal megacities and climate change, *GeoJournal*, *37*, 369, doi:10.1007/bf00814018.
Orlic, M., and Z. Pasaric (2015), Some pitfalls of the semiempirical method used to project sea level, *J. Clim.*, *28*(9), 3779–3785, doi:10.1175/jcli-d-14-00696.1.
Rahmstorf, S. (2007), A semi-empirical approach to projecting future sea-level rise, *Science*, *315*, 368–370, doi:10.1126/science.1135456.
Rahmstorf, S., M. Perrette, and M. Vermeer (2012), Testing robustness of semi-empirical sea level projections, *Clim. Dyn.*, *39*, 861–875, doi:10.1007/s00382-011-1226-7.
Rhein, M., et al (2013), Observations: Ocean, in *Climate Change 2013: The Physical Science Basis*, edited by T. F. Stocker et al. , pp. 255–316 , IPCC, Cambridge Univ. Press, Cambridge, U. K. and New York, N. Y..
Rohling, E. J., I. D. Haigh, G. L. Foster, A. P. Roberts, and K. M. Grant (2013), A geological perspective on potential future sea-level rise, *Sci. Rep.*, *3*, 3461, doi:10.1038/srep03461.
Slangen, A. B. A., M. Carson, C. A. Katsman, R. S. W. van de Wal, A. Köhl, L. L. A. Vermeersen, and D. Stammer (2014), Projecting twenty-first century regional sea-level changes, *Clim. Change*, *124*, 317–332, doi:10.1007/s10584-014-1080-9.
Song, Y., Y. Q. Yu, and P. F. Lin (2014), The hiatus and accelerated warming decades in CMIP5 simulations, *Adv. Atmos. Sci.*, *31*(6), 1316–1330, doi:10.1007/s00376-014-3265-6.
Vermeer, M., and S. Rahmstorf (2009), Global sea level linked to global temperature, *Proc. Natl. Acad. Sci. U. S. A.*, *106*(51), 21527–21532, doi:10.1073/pnas.0907765106.
Williams, R. G., P. Goodwin, A. Ridgwell, and P. L. Woodworth (2012), How warming and steric sea level rise relate to cumulative carbon emissions, *Geophys. Res. Lett.*, *39*, L19715, doi:10.1029/2012GL052771.
Williams, R. G., P. Goodwin, V. M. Rouusenov, and L. Bopp (2016), A framework to understand the transient climate response to emissions, *Environ. Res. Lett.*, *11*, 1–14, doi:10.1088/1748-9326/11/1/015003.